# Thermal–economic–environmental analysis and multi-objective optimization of an ice thermal energy storage system for gas turbine cycle inlet air cooling

Ali Shirazi [a,*], Behzad Najafi [b], Mehdi Aminyavari [c], Fabio Rinaldi [b], Robert A. Taylor [a]

[a] School of Mechanical and Manufacturing Engineering, The University of New South Wales (UNSW), Kensington, New South Wales 2052, Australia
[b] Dipartimento di Energia, Politecnico di Milano, Via Lambruschini 4, 20156 Milano, Italy
[c] Scuola di Ingegneria Industriale, Campus di Piacenza, Politecnico di Milano, Via Scalabrini 76, 29100 Piacenza, Italy

*Article history:*
Received 8 August 2013
Received in revised form
15 February 2014
Accepted 18 February 2014
Available online 4 April 2014

## 1. Introduction

Gas turbines are constant volumetric flow rate machines which, based on their design, move a given volume of air at a given shaft speed. Owing to the fact that the required air for combustion is supplied directly from the environment, weather conditions significantly impact their performance [1]. In fact, thermodynamic analyses reveal that the net output power and thermal efficiency of a gas turbine considerably decrease with increased humidity and ambient temperature [2]. This takes place due to the reduction of air density and, thus, mass flow rate [3]. Finding an alternative solution to address this issue is crucial – specifically in locations where peak electrical demand coincides with hot, humid conditions. Cooling the compressor inlet air flow is one possible solution to solve this by keeping the inlet temperature into the gas turbine constant [4]. In fact, inlet air cooling increases inlet air density and air mass flow rate, enhancing the gas turbine's power output and efficiency (especially during the summer season) [5]. Several direct inlet air cooling methods have been proposed, including: vapor compression refrigeration, absorption chiller cooling, and evaporative cooling [6]. These cooling methods can also be utilized indirectly through cold thermal energy storage (CTES) systems. In this configuration, energy is taken from the plant to cool the storage medium during off-peak hours (during the night) and later utilized for inlet air cooling during on-peak hours (during daytime) [5]. Thus, a CTES shifts the cooling input from on-peak periods (where electricity prices are high) to off-peak periods (where electricity consumption and prices are at their lowest) [7].

TES systems are divided into two major categories including sensible heat storage and latent heat storage [8]. In sensible heat storage systems, energy is stored by changing the temperature of the energy storage media (without phase change). For latent heat storage units, energy is stored by changing the phase of energy storage media at a constant temperature [9]. For the same volume and reasonable operation ranges, latent heat storage systems can store more energy than sensible heat storage systems [10]. Accordingly, for inlet air cooling, latent TES systems based

* Corresponding author. Tel.: +61 413077896.
*E-mail addresses:* a.shirazi@student.unsw.edu.au (A. Shirazi), behzad.najafi@mail.polimi.it (B. Najafi), mehdi.aminyavari@mail.polimi.it (M. Aminyavari), fabio.rinaldi@polimi.it (F. Rinaldi), Robert.Taylor@unsw.edu.au (R.A. Taylor).

## Nomenclature

| | |
|---|---|
| $A$ | heat transfer surface area ($m^2$) |
| $c_{elec}$ | electricity unit cost (US\$ $kWh^{-1}$) |
| COP | coefficient of performance |
| $c_p$ | specific heat at constant pressure (kJ $kg^{-1}$ $K^{-1}$) |
| CRF | capital recovery factor |
| $\dot{C}_{env}$ | social cost of air pollution (US\$ $s^{-1}$) |
| $\dot{C}_{tot}$ | total cost rate (US\$ $s^{-1}$) |
| $e$ | specific exergy (kJ $kg^{-1}$) |
| $\bar{e}$ | molar specific exergy (kJ $kmol^{-1}$) |
| $E$ | exergy (kWh) |
| $\dot{E}$ | exergy flow rate (kW) |
| $F$ | logarithmic mean temperature difference correction factor |
| $h$ | specific enthalpy (kJ $kg^{-1}$) |
| $i$ | interest rate (%) |
| $i_{ph}$ | melting latent heat (kJ $kg^{-1}$) |
| $k$ | specific heat ratio |
| LHV | low heating value (kJ $kg^{-1}$) |
| $\dot{m}$ | mass flow rate (kg $s^{-1}$) |
| $\dot{n}$ | molar flow rate (kmol $s^{-1}$) |
| $N$ | operational hours in a year |
| $n$ | system life time (year) |
| NTU | number of transfer units |
| $p$ | pressure (Pa), extra cost payback period (year) |
| $\dot{Q}$ | the time rate of heat transfer (kW) |
| $Q_C$ | cooling load (kWh) |
| $\dot{Q}_C$ | cooling load (kW) |
| $R_{th}$ | thermal resistance ($m^2$ K $kW^{-1}$) |
| $s$ | specific entropy (kJ $kg^{-1}$ $K^{-1}$) |
| $\bar{R}$ | universal gas constant (kJ $kmol^{-1}$ $K^{-1}$) |
| $r_p$ | pressure ratio |
| $T$ | temperature (°C or K) |
| TIT | turbine inlet temperature (K) |
| $U$ | overall heat transfer coefficient (kW $m^{-2}$ $K^{-1}$) |
| $x$ | molar fraction |
| $u$ | specific internal energy (kJ $kg^{-1}$) |
| $V$ | volume ($m^3$) |
| $\dot{W}$ | the time rate of energy transfer by work (kW) |
| $x$ | molar fraction |
| $y$ | year |
| $Z$ | capital cost (US\$) |
| $\dot{Z}$ | capital cost rate (US\$ $s^{-1}$) |

*Greek symbols*

| | |
|---|---|
| $\varepsilon$ | effectiveness |
| $\eta$ | isentropic efficiency |
| $\bar{\lambda}$ | molar fuel to air ratio |
| $\nu$ | specific volume ($m^3$ $kg^{-1}$) |
| $\rho$ | density (kg $m^{-3}$) |
| $\Phi$ | maintenance factor |
| $\phi$ | relative humidity |
| $\psi$ | exergetic efficiency |
| $\omega$ | absolute humidity (kg water vapor $kg^{-1}$ dry air) |

*Subscripts*

| | |
|---|---|
| a | air |
| AC | air cooler |
| Av | average |
| C1 | air compressor |
| C2 | refrigeration compressor |
| REC | recuperator |
| CC | combustion chamber |
| amb | ambient |
| C | cooling load |
| CH | chemical |
| ch | charging |
| GT | gas turbine |
| Cond | condenser |
| CT | cooling tower |
| cv | control volume |
| CW | chilled water |
| D | destruction |
| dc | discharging |
| EV | evaporator |
| EX | expansion valve |
| f | final, fuel |
| FP | freezing point |
| g | gas |
| i | inlet |
| int | initial |
| LMTD | logarithmic mean temperature difference |
| o | outlet |
| op | operational |
| PH | physical |
| tot | total |
| w | water |
| l | leakage |
| r | refrigerant |
| ST | ice storage tank |
| t | time |
| WB | wet-bulb |

on ice storage have received the most attention in the recent years [11].

Numerous studies have been conducted in recent years in the fields of CTES systems and gas turbine inlet air cooling techniques. Saito [12] reviewed the recent advances in the field of CTES units. In that study, various types of CTES systems were compared and their merits and drawbacks were presented. Li et al. [13] reviewed the recent development of available cold storage mediums for subzero applications and discussed their possible issues. Dincer [8] presented various technical aspects and criteria for CTES systems and their applications which showed that thermal load profiles, electrical costs, building type and occupancy are often overlooked parameters that are actually very important to system operation. Ezan et al. [14] conducted energy and exergy analyses on an ice-on-coil TES system for the charging period. The results revealed that the design parameters of the modeled TES system should be achieved by taking into account both energetic and exergetic behavior of the system. A review of the methods by which the Saudi Electric Company enhanced power generation from its combustion turbines during summer peaking hours using inlet air cooling was conducted by Al-Ibrahim and Varnham [15]. Vapor compression refrigeration inlet air cooling system using chilled water or ice thermal storage was determined to be the most suitable method for use in the desert climate of Saudi Arabia. Habeebullah [16] carried out an investigation on the economic feasibility of installing an ITES (ice thermal energy storage) system for the unique air conditioning plant of the Grand Holly Mosque of Makkah in Saudi Arabia where both operational and capital costs of the ITES system were taken into account. The results showed that employing ice storage technology under an incentive tariff model has reasonable daily savings

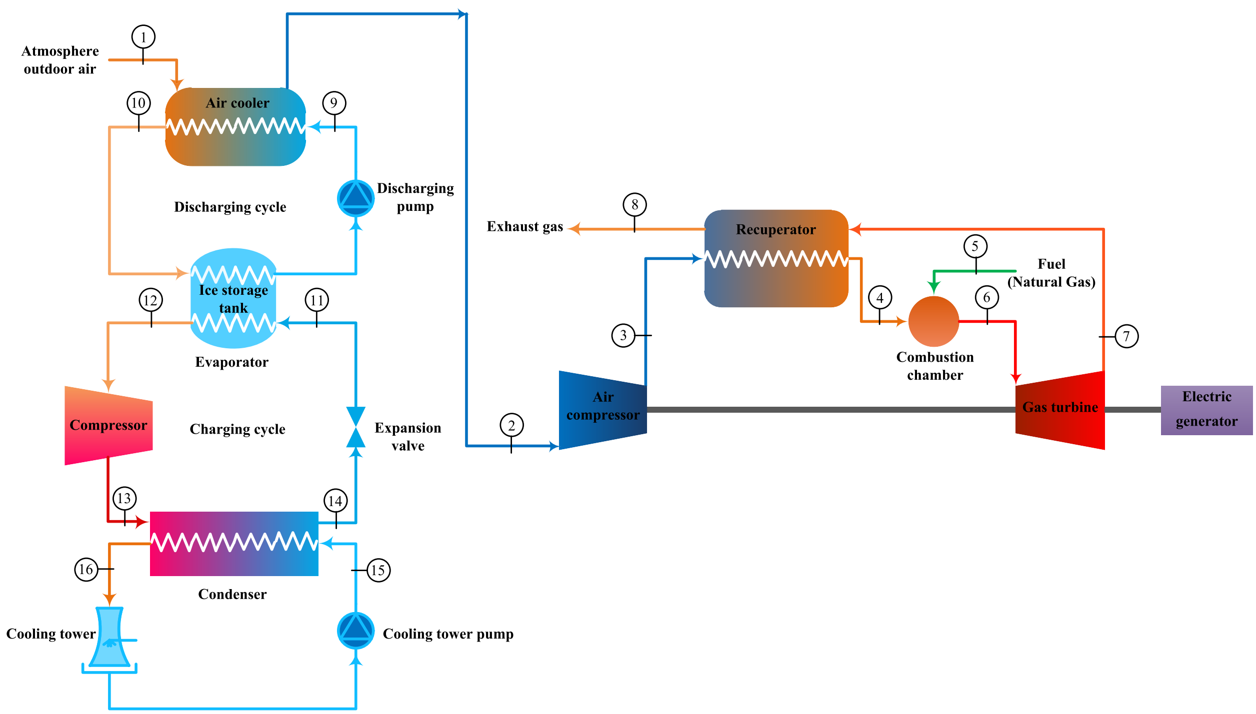


**Fig. 1.** Schematic diagram of GT power plant with inlet air cooling via ITES system.

for full storage scenario. Mohanty and Paloso [17] performed an analytical study on a GT power plant enhancement in Bangkok, Thailand, and found an 11% increase in output power was obtained using an absorption chiller for inlet air cooling. Ameri and Hejazi [18] carried out a similar feasibility study for the Chabahar gas turbine power plant in Iran. They found that the output power increased by 11.3%, while the payback period was calculated to be 4.2 years. Khaliq and Dincer [19] carried out an exergy analysis of a gas turbine cogeneration cycle with inlet air cooling and evaporative after cooling of the compressor discharge. They found that the overall pressure ratio and turbine inlet temperature have significant impacts on the energy efficiency, exergetic efficiency and power to heat ratio of the cycle. Ehyaei et al. [20] conducted exergy, economic, and environment (3E) analyses of an absorption chiller inlet air cooler for gas turbine power plants in two different Iranian climatic regions. The results showed that using the absorption chiller inlet-air cooling system in the hot months of a year is economical. A thermo-economic analysis and single-objective optimization of an ITES system for gas turbine inlet cooling was performed by Sanaye et al. [11]. They minimized the total cost of the cycle including the capital and operational costs with and without the cost corresponding to plant exergy destruction. The results showed that utilizing an ITES inlet air cooling system increased the power output and the system efficiency by 25.7% and 5.2%.

Despite the fact that there have been several investigations on gas turbine inlet air cooling with ice storage systems, few place emphasis on the exergy and economic aspects. In addition, to the author's knowledge environmental analysis and multi-objective optimization of these plants have not yet been performed.

In the present work, an ITES system for gas turbine power plant inlet air cooling has been mathematically modeled and energetic, exergetic, economic, and environmental (emissions cost) analyses have been applied on the model. Afterward, a heuristic optimization method, called multi-objective genetic algorithm, is employed in order to optimize the system design parameters while considering thermodynamic and economic objectives simultaneously. The thermodynamic objective function which should be maximized is the exergetic efficiency; while the total cost rate is the economic objective which should be minimized. The total cost rate includes the capital and operational costs of the plant together with the costs corresponding to the environmental impact of plant emissions. Employing the mentioned optimization approach, a set of optimal solutions, called Pareto front, is obtained. Utilizing the Technique for Order Preference by Similarity to an Ideal Solution (TOPSIS) method, the final optimal point is chosen from the set of non-dimensionalized objective function solutions. From this solution, the payback period is determined, which is the required time for recovering the extra costs associated with installing an ITES system.

## 2. System description

As mentioned above, a recuperated gas turbine power plant with an ITES inlet air cooling system is considered in this study. Fig. 1 illustrates the schematic diagram of the gas turbine power plant with inlet air cooling via ITES system, which has been considered in the present study. As shown in this figure, the whole plant consists of three main parts:

- The GT cycle including an air compressor ($C_1$), a recuperator (REC), a combustion chamber (CC), and a gas turbine (GT).
- The ITES charging cycle consisting of an evaporator (EV), a refrigeration compressor ($C_2$), a condenser (Cond), a cooling tower (CT), a cooling tower pump (CT pump), and an expansion valve (EX).
- The ITES discharging cycle including an air cooler (AC), a discharging pump (DC pump), and ice storage tank (ST).

In GT cycle, the cooled inlet air at node 2 is compressed by the air compressor ($C_1$) up to node 3, and is subsequently preheated in the recuperator (REC), reaching node 4. The compressed, preheated air mixes and reacts with fuel (node 5) in the combustion chamber (CC). After combustion, the hot flue gases (node 6) expand through the gas turbine (GT). Part of the generated power at the gas turbine is consumed to run the air compressor and the rest leads to the net power production. The flue gas leaving the gas turbine (node 7) goes through the recuperator and eventually, the exhaust gas is discharged to the atmosphere at node 8.

In the charging cycle of the ITES (vapor compression refrigeration) system, R134a is used as the refrigerant. This cycle is utilized to produce ice during off-peak hours when the electricity price is low (during night time). During this time, the evaporator (EV) absorbs heat ($\dot{Q}_{EV}$) from the stored water inside the storage tank at the evaporating temperature, $T_{EV}$. The refrigerant leaving the evaporator at node 12 is compressed by the refrigeration compressor ($C_2$) up to node 13 and then passes through the water-cooled condenser (Cond). The condenser then rejects heat at a rate of $\dot{Q}_{Cond}$ into the cooling tower (CT) cycle. Water flow is circulated by the cooling tower pump (CT pump) in order to cool down the water via ambient air stream entering the cooling tower. Finally, the cooled refrigerant exiting from the condenser goes through the expansion valve (EX) in order to reach the evaporator saturation pressure. This process runs continuously throughout the charging hours until enough energy is removed from the water inside the storage tank to completely convert to ice.

In the discharging cycle, a water/Glycol solution (chilled water) circulates through the store (node 10) as the secondary working fluid. This fluid is pumped by a discharging pump into the air cooler (AC) at node 9 – to cool down the inlet ambient air at node 1. It should be noted that in the present study, a full storage strategy (i.e. where the charging cycle only runs during off-peak hours) is used for modeling the ITES system.

## 3. System analysis

Mathematical modeling of the aforementioned system on the basis of thermal (energy and exergy), economic, and environmental (emissions cost) analyses is presented as follows:

### 3.1. Energy analysis

To simplify the analysis procedure, the following assumptions have been taken into consideration while developing model of the system:

- Internal distributions of temperature, pressure, and gas compositions in each component are uniform [21].
- Changes in the kinetic and potential energies of fluid streams are negligible [22,23].
- All system components, except the combustion chamber and the storage tank, are adiabatic [23].
- All system components, except the storage tank, operate under steady-state conditions [23].
- The fuel supplied to the system is assumed to be natural gas.
- Pressure drop within the connecting pipes is negligible [5].
- All cooling energy is stored in the water/ice medium [22].
- The states of the refrigerant at evaporator and condenser outlets are saturated vapor and saturated liquid, respectively [24].

#### 3.1.1. Cooling load

The ITES system capacity has important effects on the refrigeration cycle components and economic benefits. To calculate the cooling load, the total heat rejected from the inlet air flow was estimated – i.e. the heat required to change its temperature and humidity from ambient condition to 15 °C (ISO standard) and 100% relative humidity. Hence, the ITES capacity is a function of temperature and relative humidity of the ambient air.

As illustrated in Fig. 2, the cooling process at the air cooler consists of two steps, which are sensible heat rejection (a–b) and latent heat rejection (b–c) absorbed by the chilled water passing through the air cooler. Thus, the total cooling load can be calculated using the energy balance at the air cooler, which is determined as follows:

$$\dot{Q}_C = \dot{m}_a(h_1 - h_2) = \dot{m}_a\left[(h_a - h_b) + h_{fg}(\omega_a - \omega_c)\right] \tag{1}$$

$$\omega = 0.622 \times \frac{\phi \times p_{ws}}{p_{atm} - \phi \times p_{ws}} \tag{2}$$

where $p_{ws}$ is the water vapor saturation pressure at the dry bulb temperature and $\phi$ is the relative humidity. $p_{ws}$ is a function of temperature and can be estimated as follows [25]:

$$p_{ws} = \frac{C_1}{T} + C_2 + C_3T + C_4T^2 + C_5T^3 + C_6\ln(T) \tag{3}$$

Owing to the fact that part of the stored cooling energy is lost due to the heat transfer between the storage tank and its surroundings, a thermal efficiency ($\eta_{ST}$) is defined for the storage tank. In this paper, the shape of the storage tank is assumed to be cylindrical (with diameter equal to the height) to minimize the heat leakage rate [7]. Therefore, the cooling energy which should be stored in the storage tank ($Q_{ST}$, kWh) is obtained by

$$Q_{ST} = \frac{\left(\dot{Q}_C \times t_{dc}\right)}{\eta_{ST}} \tag{4}$$

$$\eta_{ST} = \frac{Q_{ST} - Q_{l,ch} - Q_{l,dc}}{Q_{ST}} = 1 - \left(\frac{Q_{l,ch} + Q_{l,dc}}{Q_{ST}}\right) \tag{5}$$

where $t_{dc}$ is the discharging time when inlet air cooling is required, while $Q_{l,ch}$, and $Q_{l,dc}$ are the heat leakage rates of storage tank during charging and discharging processes, which are obtained from Eqs. (36) and (43) respectively.

#### 3.1.2. Gas turbine cycle

*3.1.2.1. Air compressor.* The isentropic efficiency of the air compressor ($\eta_{C1}$) is defined as

$$\eta_{C1} = \frac{h_{3,s} - h_2}{h_3 - h_2} \tag{6}$$

The temperature of working fluid at air compressor outlet ($T_3$) can be determined by

$$T_3 = T_2\left[1 + \frac{r_{p,C1}^{\left(\frac{k-1}{k}\right)} - 1}{\eta_{C1}}\right] \tag{7}$$

Applying the energy balance equation, the air compressor power consumption ($\dot{W}_{C1}$) is calculated as

$$\dot{W}_{C1} = \dot{m}_a(h_3 - h_2) \tag{8}$$

*3.1.2.2. Recuperator.* The recuperator was considered to be a plate-fin heat exchanger with cross flow configuration. $\varepsilon$-NTU method is used to determine the specifications of the recuperator. The effectiveness of the recuperator ($\varepsilon$) is defined by Ref. [26]:

$$\varepsilon = \begin{cases} \dfrac{T_{h,i} - T_{h,o}}{T_{h,i} - T_{c,i}}, & \text{if } C_h < C_c \\[2ex] \dfrac{T_{c,o} - T_{c,i}}{T_{h,i} - T_{c,i}}, & \text{if } C_c < C_h \end{cases} \tag{9}$$

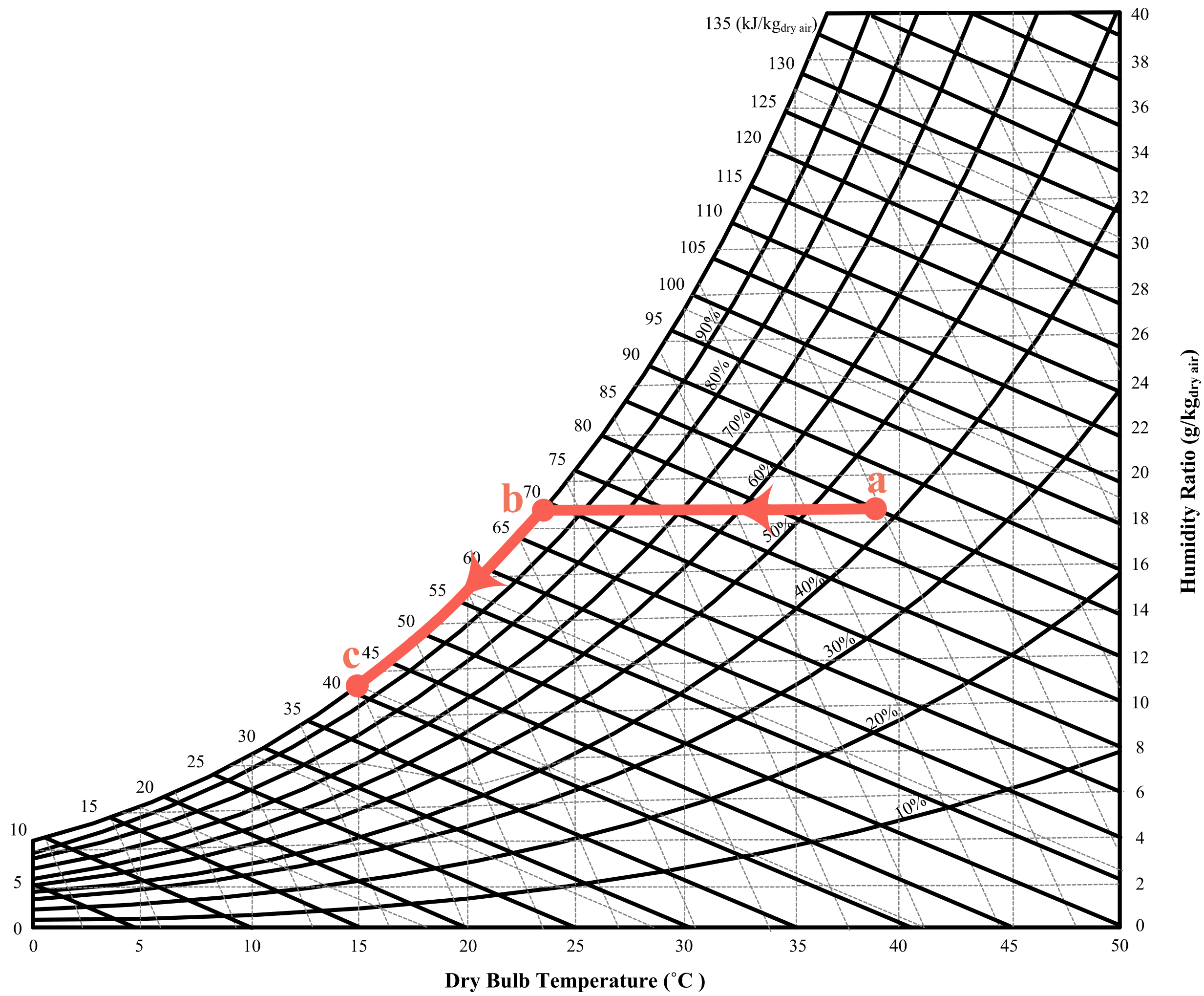


**Fig. 2.** Air cooling process in a psychometric chart (a: ambient condition; b: dew point; c: final condition).

where $T_{h,i}$ and $T_{h,o}$ are inlet and outlet temperatures of hot fluid, $T_{c,i}$ and $T_{c,o}$ are inlet and outlet temperatures of cold fluid, and finally $C_c$ and $C_h$ are heat capacity rate of cold and hot fluids.

The energy balance equation for the recuperator can be expressed as follows:

$$\dot{Q}_{REC} = \dot{m}_3(h_4 - h_3) = \dot{m}_7(h_7 - h_8) \tag{10}$$

The heat transfer surface area of recuperator ($A_{REC}$) can be determined as [26]

$$A_{REC} = \frac{\dot{Q}_{REC}}{U_{REC} \times F_{REC} \times \Delta T_{LMTD,REC}} \tag{11}$$

where

$$\Delta T_{LMTD,REC} = \frac{(T_8 - T_3) - (T_7 - T_4)}{\ln\left(\frac{T_8 - T_3}{T_7 - T_4}\right)} \tag{12}$$

*3.1.2.3. Combustion chamber.* The energy balance equation for the combustion chamber is written as

$$\dot{m}_4 h_4 + \dot{m}_5 \text{LHV} = \dot{m}_6 h_6 + (1 - \eta_{CC})\dot{m}_5 \text{LHV} \tag{13}$$

where $\eta_{CC}$ is the combustion chamber efficiency, and LHV is the fuel lower heating value.

The chemical reaction occurring inside the combustion chamber can be formulated as

$$\begin{aligned}&\bar{\lambda} C_{x_1} H_{y_1} + (x_{O_2} O_2 + x_{N_2} N_2 + x_{H_2O} H_2O + x_{CO_2} CO_2 + x_{Ar} Ar)\\ &\rightarrow y_{CO_2} CO_2 + y_{N_2} N_2 + y_{O_2} O_2 + y_{H_2O} H_2O + y_{NO} NO\\ &\quad + y_{CO} CO + y_{Ar} Ar\end{aligned} \tag{14}$$

where

$$y_{CO_2} = \left(\bar{\lambda} \times x_1 + x_{CO_2} - y_{CO}\right) \tag{15}$$

$$y_{N_2} = x_{N_2} - y_{NO} \tag{16}$$

$$y_{H_2O} = x_{H_2O} + \frac{\bar{\lambda} \times y_1}{2} \tag{17}$$

$$y_{O_2} = x_{O_2} - \bar{\lambda} \times x_1 - \frac{\bar{\lambda} \times y_1}{4} - \frac{y_{CO}}{2} - \frac{y_{NO}}{2} \tag{18}$$

$$y_{Ar} = x_{Ar} \tag{19}$$

$$\bar{\lambda} = \frac{\dot{n}_f}{\dot{n}_a} \tag{20}$$

*3.1.2.4. Gas turbine.* The flue gas temperature at the gas turbine outlet ($T_7$) can be determined by

$$T_7 = T_6\left\{1 - \eta_{GT}\left[1 - \left(\frac{p_6}{p_7}\right)^{\frac{1-k_g}{k_g}}\right]\right\} \tag{21}$$

The generated mechanical power of the gas turbine ($\dot{W}_{GT}$) is determined as

$$\dot{W}_{GT} = \dot{m}_6(h_6 - h_7) \tag{22}$$

where

$$\dot{m}_6 = \dot{m}_4 + \dot{m}_5 \tag{23}$$

Finally, the net generated power is calculated as follows:

$$\dot{W}_{net} = \dot{W}_{GT} - \dot{W}_{C1} \tag{24}$$

### 3.1.3. ITES system

*3.1.3.1. Charging (freezing) cycle.* In the charging process, a vapor compression refrigeration system was used to make and store ice in the storage tank. Assuming that the total amount of stored energy ($Q_{ST}$) is known, the evaporator heat transfer rate is defined as follows:

$$\dot{Q}_{EV} = \frac{Q_{ST}}{t_{ch}} \tag{25}$$

where $t_{ch}$ is the charging time (h). As an ice-on-coil external melt ice storage tank was utilized in this paper, the evaporator was assumed to be the serpentine coils mounted inside the storage tank.

Therefore, the refrigerant mass flow rate is

$$\dot{m}_r = \frac{\dot{Q}_{EV}}{h_{12} - h_{11}} \tag{26}$$

The refrigeration compressor power consumption is calculated by

$$\dot{W}_{C2} = \dot{m}_r(h_{13} - h_{12}) = \frac{\dot{m}_r(h_{13s} - h_{12})}{\eta_{C2}} \tag{27}$$

where $\eta_{C2}$ is the refrigeration compressor isentropic efficiency estimated from Ref. [27]:

$$\eta_{C2} = 0.85 - 0.46667\left(\frac{p_{13}}{p_{12}}\right) \tag{28}$$

It should be noted that the average clearance of 10% has been considered for the refrigeration compressor [28] and the resulting volumetric efficiency has been taken into account. The condenser heat transfer rate is obtained as follows:

$$\dot{Q}_{Cond} = \dot{m}_r(h_{13} - h_{14}) \tag{29}$$

The mass flow rate of water flow inside the cooling tower can be estimated from Ref. [29]:

$$\dot{m}_{CT} = 43.2 \times 10^{-3}\dot{Q}_{Cond} \tag{30}$$

The coefficient of performance (COP) of refrigeration system is defined as

$$COP = \frac{\dot{Q}_{EV}}{\dot{W}_{C2}} \tag{31}$$

The heat transfer surface area of the evaporator and condenser can be estimated by Ref. [26]:

$$A_{EV} = \frac{NTU \times (\dot{m}c_p)_{min}}{U_{EV}} \tag{32}$$

$$A_{Cond} = \frac{\dot{Q}_{Cond}}{U_{Cond} \times F_{Cond} \times \Delta T_{LMTD,Cond}} \tag{33}$$

It should be mentioned that the condenser modeled in this paper is a shell and tube heat exchanger with a counter flow configuration where cooling water passes through the tube bundles while refrigerant flows into the shell. More details on calculation of the overall heat transfer coefficients of the evaporator and condenser can be found in Ref. [26]. Cooling tower pump power consumption ($\dot{W}_{pump,CT}$) is calculated as [26]

$$\dot{W}_{pump,CT} = \frac{\dot{m}_{CT} \times \Delta p_i}{\rho_w \times \eta_{pump}} \tag{34}$$

where $\Delta p_i$ and $\eta_{pump}$ are cooling tower water side pressure drop and pump isentropic efficiency.

Furthermore, the electrical power consumption of cooling tower fan ($\dot{W}_{fan,CT}$) is obtained by Ref. [30]:

$$\dot{W}_{fan,CT} = \frac{\Delta p_a \times \dot{V}_a}{\eta_{fan}\eta_m} \tag{35}$$

where $\Delta p_a$, $\dot{V}_a$, $\eta_{fan}$, and $\eta_m$ are the cooling tower air side pressure drop, volumetric flow rate of air, fan isentropic efficiency, and fan motor efficiency respectively.

For a constant temperature distribution within the storage tank, the amount of heat leakage will be a function of inner temperature of the tank, ambient temperature, storage tank heat transfer surface area, and its thermal resistance. During the charging process, the temperature of the tank is $T_{ST}$. Therefore, the amount of heat leakage of the storage tank during charging process ($Q_{l,ch}$) is expressed as

$$Q_{l,ch} = A_{ST}\frac{T_{amb} - T_{ST}}{R_{th}}t_{ch} \tag{36}$$

where $T_{amb}$, $A_{ST}$ and $R_{th}$ are the ambient temperature, storage tank heat transfer surface area, and thermal resistance of the storage tank. The heat transfer surface area of the storage tank ($A_{ST}$) should be estimated to evaluate the amount of storage tank heat leakage. The following relations are used to find the storage tank volume, and consequently, its area [22]:

$$V_{ST} = \frac{3600Q_{ST}}{\rho_w c_{p,w}(T_{dc} - T_{FP,w}) + \rho_w i_{ph} + \rho_{ice}c_{p,ice}(T_{FP,w} - T_{ST})} \tag{37}$$

$$A_{ST} = 6\pi\left(\frac{V_{ST}}{2\pi}\right)^{\frac{2}{3}} \tag{38}$$

*3.1.3.2. Discharging (melting) cycle.* In discharging cycle, the storage tank is used for cooling the chilled water. Then, chilled water is pumped into the AC to cool the inlet ambient air stream. The AC was considered to be a finned tube compact heat exchanger with a cross flow configuration.

Calculating the required cooling load from Eq. (1), the air cooler heat transfer surface area can be obtained by Ref. [26]:

$$A_{AC} = \frac{\dot{Q}_C}{U_{AC} \times F_{AC} \times \Delta T_{LMTD,AC}} \tag{39}$$

where

$$\Delta T_{LMTD,AC} = \frac{(T_2 - T_9) - (T_1 - T_{10})}{\ln\left(\frac{T_2 - T_9}{T_1 - T_{10}}\right)} \tag{40}$$

More details on calculation of the overall heat transfer coefficient of the air cooler can be found in Ref. [11].

The power consumption of AC fan ($\dot{W}_{fan,AC}$) is estimated as [26]

$$\dot{W}_{fan,AC} = \frac{\left(\Delta p_o + \Delta p_{fan}\right) \times \dot{V}_a}{\eta_{fan}} \tag{41}$$

where $\Delta p_o$, $\Delta p_{fan}$, $\dot{V}_a$, and $\eta_{fan}$ are the AC air side pressure drop, fan pressure drop, air volume flow rate, and fan isentropic efficiency, respectively

The pumping power consumption during discharging process ($\dot{W}_{pump,dc}$) is obtained by Ref. [26]:

$$\dot{W}_{pump,dc} = \frac{\dot{m}_{CW} \times \Delta p_i}{\rho_{CW} \times \eta_{pump}} \tag{42}$$

where $\dot{m}_{CW}$, $\Delta p_i$, and $\eta_{pump}$ are chilled water mass flow rate, chilled water (cold stream) side pressure drop at AC, and the pump isentropic efficiency, respectively.

Finally, the amount of heat leakage of the storage tank during discharging process is

$$Q_{l,dc} = A_{ST}\frac{T_{amb} - T_{dc}}{R_{th}}t_{dc} \tag{43}$$

where $T_{dc}$ is the discharging temperature.

### 3.2. Exergy analysis

Exergy is defined as the maximum obtainable work that a system can yield in a given state when it comes down to the environment conditions. The method of exergy analysis is based on the second law of thermodynamics and enables designers to identify location, cause, and true magnitude of wastes and losses in thermal systems [27].

Applying the first and second laws of thermodynamics, the exergy balance equation for a closed system can be written as

$$E_f - E_i = E^Q - E^W - E_D \tag{44}$$

where $E^Q$, $E^W$ and $E_D$ are the exergy transfer associated with heat transfer, net useful work, and exergy destruction. The term $(E_f - E_i)$ is the exergy change in the closed system which can be obtained by Ref. [31]:

$$E_f - E_i = m\left[\left(u_f - u_i\right) + p_0\left(v_f - v_i\right) - T_0\left(s_f - s_i\right)\right] \tag{45}$$

Furthermore, the steady state form of exergy balance equation for a control volume can be expressed as follows:

$$\frac{dE_{cv}}{dt} = \sum_j \dot{E}_j^Q - \dot{E}^W + \sum_i \dot{E}_i - \sum_e \dot{E}_e - \dot{E}_D = 0 \tag{46}$$

where $\dot{E}_i$ and $\dot{E}_e$ are the exergy transfer rate at control volume inlets and outlets, $\dot{E}_D$ is the exergy destruction rate due to irreversibilities, $\dot{E}^W$ is the rate of exergy transfer by work, and $\dot{E}^Q$ is the rate of exergy transfer by heat transfer, respectively.

In absence of electromagnetic, electric, nuclear, and surface tension effects and assuming a negligible change in potential and kinetic energy, the exergy flow rate of the system is divided into two parts – physical and chemical exergy [27,31]:

$$\dot{E} = \dot{E}^{PH} + \dot{E}^{CH} \tag{47}$$

The physical exergy can be determined by

$$\dot{E}^{PH} = \dot{m}[(h - h_0) - T_0(s - s_0)] \tag{48}$$

The chemical exergy of gaseous mixtures can be determined by

$$\dot{E}^{CH} = \dot{n}\left[\sum_k x_k \bar{e}_k^{CH} + \bar{R}T_0 \sum_k x_k \ln x_k\right] \tag{49}$$

Furthermore, the second law efficiency (exergetic efficiency) is calculated as follows:

$$\psi = \frac{\dot{E}_{out}}{\dot{E}_{in}} = 1 - \frac{\dot{E}_D}{\dot{E}_{in}} \tag{50}$$

Exergetic efficiency, $\psi$, indicates how much exergy has been converted into useful work. In this paper, the exergy flow rate of each stream line is calculated at all states and the changes in exergy are determined for each system component. The exergy destruction rate for each component of the whole system is summarized in Table 1.

### 3.3. Economic analysis

Both thermodynamic and economic aspects are important in analysis and optimization of energy systems. In the present work, the economic analysis takes into account both the capital and maintenance costs of the system components and the operational cost of the plant which includes the costs of electricity and fuel consumption.

#### 3.3.1. Capital, maintenance, and operational costs

The considered cost functions for all components of the plant are given in Table 2 [32–37]. Accordingly, the capital cost of each component ($Z_k$) is determined and in order to calculate the corresponding cost per unit of time ($\dot{Z}_k$) the following relation is employed:

$$\dot{Z}_k = \frac{Z_k \times CRF \times \Phi}{N \times 3600} \tag{51}$$

where $\Phi$ is the maintenance factor, $N$ is the annual operational hours of the system, and CRF is the capital recovery factor which,

**Table 1**
The exergy destruction rate for each component of the plant.

| Component | Exergy destruction rate |
|---|---|
| Air cooler | $\dot{E}_{D,AC} = (\dot{E}_1 + \dot{E}_9) - (\dot{E}_2 + \dot{E}_{10})$ |
| Air compressor | $\dot{E}_{D,C1} = \dot{E}_2 - \dot{E}_3 + \dot{W}_{C1}$ |
| Recuperator | $\dot{E}_{D,Rec} = (\dot{E}_3 + \dot{E}_7) - (\dot{E}_4 + \dot{E}_8)$ |
| Combustion chamber | $\dot{E}_{D,CC} = -((1 - \eta_{CC})\dot{m}_5 LHV)\left(1 - \frac{T_0}{T_{CC}}\right) + (\dot{E}_4 + \dot{E}_5) - \dot{E}_6$ |
| Gas turbine | $\dot{E}_{D,GT} = \dot{E}_6 - \dot{E}_7 - \dot{W}_{GT}$ |
| Ice storage tank | $\dot{E}_{D,ST} = \frac{E^Q_{ST,ch} - (E_f - E_i)_{ST,ch}}{t_{ch}} + \frac{E^Q_{ST,dc} - (E_f - E_i)_{ST,dc}}{t_{dc}} + (\dot{E}_{10} - \dot{E}_9) + \dot{E}^Q$ |
| Evaporator | $\dot{E}_{D,EV} = (\dot{E}_{11} - \dot{E}_{12}) + \dot{E}^Q_{EV} = (\dot{E}_{11} - \dot{E}_{12}) + \dot{Q}_{EV}\left(1 - \frac{T_0}{T_{EV}}\right)$ |
| Refrigeration compressor | $\dot{E}_{D,C2} = \dot{E}_{12} - \dot{E}_{13} + \dot{W}_{C2}$ |
| Condenser | $\dot{E}_{D,Cond} = (\dot{E}_{13} + \dot{E}_{15}) - (\dot{E}_{14} + \dot{E}_{16})$ |
| Expansion valve | $\dot{E}_{D,EX} = \dot{E}_{14} - \dot{E}_{11}$ |
| Cooling tower | $\dot{E}_{D,CT} = \dot{E}_{16} - \dot{E}_{15}$ |

**Table 2**
The cost functions in terms of thermodynamic parameters for the system components [32–37].

| System component | Capital cost function |
|---|---|
| Air compressor | $Z_{C1} = \frac{39.5\times\dot{m}_a}{0.9-\eta_{C1}}\left(\frac{p_2}{p_1}\right)\ln\left(\frac{p_2}{p_1}\right)$ |
| Recuperator | $Z_{REC} = 2290(A_{REC})^{0.6}$ |
| Combustion chamber | $Z_{CC} = \left(\frac{46.08\dot{m}_a}{0.995-\frac{p_6}{p_4}}\right)\left[1+\exp(0.018T_6-26.4)\right]$ |
| Gas turbine | $Z_{GT} = \frac{479.34\dot{m}_g}{0.92-\eta_{GT}}\ln\left(\frac{p_6}{p_7}\right)\left[1+\exp(0.036T_6-54.4)\right]$ |
| Air cooler | $Z_{AC} = 24,202\times A_{AC}^{0.4162}$ |
| Pump | $Z_{pump} = 705.48\times\dot{W}_{pump}^{0.71}\left(1+\frac{0.2}{1-\eta_{pump}}\right)$ |
| Ice storage tank | $Z_{ST} = 8.67\times10^{[2.9211\exp(0.1416\times\log V_{ST})]}$ |
| Evaporator | $Z_{EV} = 16,648.3\times A_{EV}^{0.6123}$ |
| Refrigeration compressor | $Z_{C2} = 10,089.9\times\dot{W}_{C2}^{0.46}$ |
| Expansion valve | $Z_{EX} = 114.5\times\dot{m}_r$ |
| Condenser | $Z_{Cond} = (516.621\times A_{Cond})+268.45$ |
| Cooling tower | $Z_{CT} = 746.749\times(\dot{m}_{CT})^{0.79}(\Delta T_{CT})^{0.57}(T_{in,CT}-T_{WT,out})^{-0.9924}(0.022T_{WB,out}+0.39)^{2.447}$ |

based on the interest rate ($i$) and the system life time ($n$), is obtained using the following relation [31]:

$$\mathrm{CRF} = \frac{i(1+i)^n}{(1+i)^n-1} \tag{52}$$

Furthermore, the operational cost associated with the electricity and fuel consumption of the system ($\dot{C}_{op}$) can be calculated as

$$\dot{C}_{op} = \dot{C}_{elec}+\dot{C}_f = \left[\left(\dot{W}_{C2}+\dot{W}_{pump,CT}+\dot{W}_{fan,CT}\right)\times\frac{c_{elec,off-peak}}{3600}\right] + \left[\left(\dot{W}_{fan,AC}+\dot{W}_{pump,dc}\right)\times\frac{c_{elec,on-peak}}{3600}\right] + \left[c_f\times\left(\frac{\mathrm{LHV}}{1000}\right)\times\dot{m}_f\right] \tag{53}$$

where $c_{elec,off\text{-}peak}$, $c_{elec,on\text{-}peak}$ are the unit costs of electricity for off-peak and on-peak hours respectively, while $c_f$ is the unit cost of fuel.

### 3.3.2. The payback period

The payback period is the time required for recovering the initial investment costs of a system from the net received revenue of the system [31]. Using an ITES system for inlet air cooling of gas turbine cycle imposes additional expenses which consist of investment, maintenance and operational costs of installing the ITES system. These additional costs can be compensated over time with the addition income received from the more improved system.

Assuming $E_C$ is the sum of capital cost of ITES system (including the air cooler, refrigeration system and storage tank), its corresponding electricity consumption cost, and the cost associated with fuel consumption, the worth of this investment in the $p$th year of operation of the plant ($E_{C,p}$) is estimated by

$$E_{C,p} = \left.\sum_k Z_k\right)(1+i)^p + \sum_{m=1}^{p}\dot{C}_{elec}\times N\times3600(1+i)^{p-m} \times\sum_{m=1}^{p}c_f\times\left(\frac{\mathrm{LHV}}{1000}\right)\times\Delta\dot{m}_f(1+i)^{p-m} \tag{54}$$

At the same time, the worth of net income received from selling the augmented generated electricity due to inlet air cooling in the $p$th year is calculated as

$$E_p = \sum_{m=1}^{p}\Delta\dot{W}\times N\times c_{elec}(1+i)^{p-m} \tag{55}$$

where $c_{elec}$ is the unit cost of electricity for selling. Utilizing Eqs. (54) and (55) and the Newton–Raphson numerical method, the payback period of the ITES system ($p$) can be obtained.

### 3.4. Environmental analysis

Recently, environmental impact has been one of the major concerns in analysis of energy systems. Accordingly, the present study accounts for carbon monoxide (CO), nitrogen monoxide ($NO_x$), and carbon dioxide ($CO_2$) emissions in the total cost rate of the system.

The amounts of CO and $NO_x$ production within the combustion chamber, based on the residence time in the combustion zone ($\tau$) and the primary zone combustion temperature ($T_{pz}$) can be determined by Ref. [38]:

$$m_{CO} = \frac{0.179\times10^9\times\exp\left(\frac{7800}{T_{pz}}\right)}{p^2\tau\left(\frac{\Delta p}{p}\right)^{0.5}} \tag{56}$$

$$m_{NO_x} = \frac{0.15\times10^{16}\times\tau^{0.5}\exp\left(\frac{-71,100}{T_{pz}}\right)}{p^{0.05}\left(\frac{\Delta p}{p}\right)^{0.5}} \tag{57}$$

while the emission amount is found in terms of grams per kilogram of fuel and $\Delta p/p$ indicates the non-dimensional pressure drop in the combustion chamber. Detailed relations for determining the $\tau$ and $T_{pz}$ are given in Refs. [38,39].

It is noteworthy that based on combustion equation (Eq. (15)) in the combustion chamber, the amount of $CO_2$ emission is determined.

## 4. System optimization

### 4.1. Definition of the objective functions

Multi-objective optimization is a realistic model for many real-world problems dealing with conflicting objectives. The advantage of this process is that it can simultaneously optimize any number of conflicting objectives with several equality and inequality constraints. Apparently, the optimum solution for multi-objective optimization is not unique. Hence, a logical solution to a multi-objective problem is to investigate a set of non-dominated solutions, each of which satisfies the objectives at an acceptable level [40,41]. After determining the set of solutions, the 'Pareto optimal set', a decision-maker must decide which of the achieved design vectors is suitable for the specific project [42,43]. Considering $k$ objectives to be optimized, a multi-objective optimization problem can be defined as follows:

$$\text{minimize or maximize } [f_1(\mathbf{x}), f_2(\mathbf{x}), \ldots, f_k(\mathbf{x})]^{\mathrm{T}}$$

$$g(\mathbf{x}) \le 0$$

$$h(\mathbf{x}) = 0$$

$$\mathbf{x}_{\mathrm{l}} \le \mathbf{x} \le x_{\mathrm{u}}$$

where $f_k$ is the $k$th objective function, $g$ and $h$ stand for the inequality and equality constraints, and $\mathbf{x}$ denotes the design parameters.

In the present work, the exergetic efficiency and the total cost rate of the system are considered as the objective functions of the multi-objective optimization procedure, which should be maximized and minimized, respectively. These objective functions can be expressed using the following relations:

#### 4.1.1. Exergetic efficiency (objective function I)

$$\psi_{\mathrm{tot}} = \frac{\dot{E}_{\mathrm{out}}}{\dot{E}_{\mathrm{in}}} = \left(\frac{\dot{W}_{\mathrm{net}}}{\dot{W}_{\mathrm{fan,AC}} + \dot{W}_{\mathrm{pump,dc}} + \dot{W}_{\mathrm{C2}} + \dot{W}_{\mathrm{pump,CT}} + \dot{W}_{\mathrm{fan,CT}} + \dot{m}_{\mathrm{f}} e_{\mathrm{f}}^{\mathrm{CH}}}\right)$$
$$= 1 - \left(\frac{\dot{E}_{\mathrm{D,tot}}}{\dot{W}_{\mathrm{fan,AC}} + \dot{W}_{\mathrm{pump,dc}} + \dot{W}_{\mathrm{C2}} + \dot{W}_{\mathrm{pump,CT}} + \dot{W}_{\mathrm{fan,CT}} + \dot{m}_{\mathrm{f}} e_{\mathrm{f}}^{\mathrm{CH}}}\right) \quad (58)$$

where $\dot{E}_{\mathrm{D,tot}}$ is the sum of exergy destruction rate of system components.

#### 4.1.2. Total cost rate (objective function II)

$$\dot{C}_{\mathrm{tot}} = \sum_k \dot{Z}_k + \dot{C}_{\mathrm{op}} + \dot{C}_{\mathrm{env}} \quad (59)$$

where

$$\dot{C}_{\mathrm{env}} = c_{\mathrm{CO}}\dot{m}_{\mathrm{CO}} + c_{\mathrm{NO}_x}\dot{m}_{\mathrm{NO}_x} + c_{\mathrm{CO}_2}\dot{m}_{\mathrm{CO}_2} \quad (60)$$

In Eq. (60), $\dot{m}_{\mathrm{CO}}$, $\dot{m}_{\mathrm{NO}_x}$, and $\dot{m}_{\mathrm{CO}_2}$ are the exhaust mass flow rates of carbon monoxide, nitrogen monoxide, and carbon dioxide respectively, while $c_{\mathrm{CO}}$, $c_{\mathrm{NO}_x}$, and $c_{\mathrm{CO}_2}$ are their corresponding damage unit costs.

### 4.2. Design parameters and constraints

The following design parameters are chosen for optimization of the modeled system: the air compressor pressure ratio ($r_{\mathrm{p,C1}}$), the isentropic efficiencies of air compressor ($\eta_{\mathrm{C1}}$) and gas turbine ($\eta_{\mathrm{GT}}$), the gas turbine inlet temperature (TIT), the storage temperature inside the storage tank ($T_{\mathrm{ST}}$), the refrigerant saturation temperature at evaporator ($T_{\mathrm{EV}}$) and condenser ($T_{\mathrm{Cond}}$).

The aforementioned design parameters and their range of variation as well as the system constraints are listed in Table 3.

### 4.3. Genetic algorithm

The genetic algorithm (GA) method is a semi-stochastic method based on an analogy with Darwin's laws of natural selection [44]. In this algorithm, a solution vector (design parameters vector) is called a chromosome and is made of discrete units called genes. These genes control features of the chromosomes. GAs are well-suited to solve multi-objective optimization problems [44]. This algorithm has been widely employed for optimization of thermal systems to date [7,45–48].

New generations of solutions are generated from existing ones through two operators, crossover and mutation. As the search evolves, the population converges, and eventually is dominated by a set of solutions called the Pareto optimal set.

In the present work, the genetic algorithm method is employed to optimize the objective functions presented in Eqs. (58) and (59).

## 5. Case study

In the present study, the ITES system, for inlet air cooling purposes, is considered to be installed in the Fars gas turbine power plant in Shiraz, a city in the southern part of Iran. This plant consists of a Siemens/Westinghouse gas turbine unit model V64.3 with 62.3 MW nominal power output and 35.2% thermal efficiency at ISO conditions. The input parameters listed in Table 4 are taken into consideration for simulation of the GT cycle with inlet air cooling via ITES system. Figs. 3 and 4 illustrate the profiles of minimum and maximum values of ambient temperature and relative humidity over a year in Shiraz [49].

In the present study, the inlet air cooling process is conducted from March to November in the Fars power plant. The average required cooling load is calculated for each month based on Eq. (1), which is shown in Fig. 5. The maximum required cooling load is 6805.8 kW in July and its minimum value is 352.2 kW in March. It is assumed that the charging cycle operates during off-peak hours (from 12 AM to 8 AM (8 h)) and the discharging cycle operates during on-peak hours (from 8 AM to 5 PM (9 h)).

The thermodynamic properties of refrigerant used in the modeling of vapor compression refrigeration cycle (R134a) are obtained from an in-house developed software according to ASHARE Handbook [25], and thermodynamic and chemical properties of other working fluids are derived from JANAF tables [50]. For the exergy calculation, the atmospheric condition is considered as the dead state. Thus, $T_0$ is equal to ambient temperature (varying according to Fig. 3) and $P_0$ is the ambient pressure. The corresponding unit costs of generated electricity ($c_{\mathrm{elec}}$) and the fuel ($c_{\mathrm{f}}$) are 0.06 US\$ kWh$^{-1}$ and 0.004 US\$ MJ$^{-1}$ (0.12 US\$ m$^{-3}$), respectively [23]. Moreover, the electricity unit costs of on-peak and off-peak hours are 0.09 US\$ kWh$^{-1}$ and 0.06 US\$ kWh$^{-1}$, respectively [7]. The unit damage costs associated with CO ($c_{\mathrm{CO}}$), $NO_x$ ($c_{\mathrm{NO}_x}$), and $CO_2$ ($c_{\mathrm{CO}_2}$) are considered to be 0.02086 US\$ kg$^{-1}$ CO, 6.853 US\$ kg$^{-1}$ $NO_x$, and 0.0224 US\$ kg$^{-1}$ $CO_2$, respectively [51,52].

**Table 3**
List of constraints for system optimization and the range of variation of design parameters.

| Constraints | Reason |
|---|---|
| $2 < r_{p,C1} < 16$ | Typical technology and commercial availability |
| $0.6 < \eta_{C1} < 0.9$ | Typical technology and commercial availability |
| $0.6 < \eta_{GT} < 0.95$ | Typical technology and commercial availability |
| $900\ K < TIT < 1550\ K$ | The material limit of available technology |
| $-10\ ^\circ C < T_{ST} < 0\ ^\circ C$ | Typical data for refrigeration systems |
| $-30\ ^\circ C < T_{EV} < 0\ ^\circ C$ | Minimum and maximum refrigerant saturation temperature in the evaporator for a wide range of applications |
| $(T_{WB,out} + 5)\ ^\circ C < T_{Cond} < 60\ ^\circ C$ | Minimum and maximum refrigerant saturation temperature in the condenser for a wide range of applications |
| $T_8 > 400\ K$ | To avoid formation of sulfuric acid in exhaust gases |
| $T_7 > T_8$ | For heat exchange between hot and cold streams in the recuperator |
| $T_7 > T_4$ | For heat exchange between hot and cold streams in the recuperator |
| $T_8 > T_3$ | For heat exchange between hot and cold streams in the recuperator |
| $T_{EV} < T_{ST}$ | For heat transfer between the evaporator and the storage tank |
| $T_{FP,Glycol} < T_{ST}$ | To avoid icing water/glycol solution in the discharging cycle |

To determine the CRF (Eq. (52)), the approximate life time of the system ($n$), the maintenance factor ($\Phi$), and the annual interest rate (i) are considered as 20 years, 1.06, and 14% [53]. The annual operational hours of the gas turbine, ITES charging and discharging cycles are 8640 h, 2160 h, and 2430 h.

**Table 4**
Input parameters used for simulation of GT cycle with inlet air cooling via ITES system.

| Parameter | Value |
|---|---|
| *GT–ITES cycle* | |
| Recuperator effectiveness ($\varepsilon$) | 0.88 |
| Combustion chamber efficiency ($\eta_{CC}$) | 0.98 |
| Chilled water temperature at air cooler inlet ($T_9$, °C) | 5 |
| Chilled water temperature at air cooler outlet ($T_{10}$, °C) | 12 |
| Air temperature at air compressor inlet ($T_2$, °C) | 15 |
| Relative humidity at air compressor inlet (%) | 100 |
| Storage tank thermal resistance ($R_{th}$, $m^2\ K\ kW^{-1}$) | 1980 |
| Refrigeration compressor isentropic efficiency ($\eta_{C2}$) | 0.88 |
| Pump efficiency ($\eta_{pump}$) | 0.83 |
| *Pressure losses* | |
| Recuperator (%) | 4 |
| Air cooler (%) | 4 |
| Condenser (%) | 4 |
| Combustion chamber (%) | 5 |
| *Fuel (natural gas) properties* [27] | |
| Composition (percent by volume) | $CH_4$ (95%), $C_2H_6$ (2.5%), $CO_2$ (1%), $N_2$ (1.5%) |
| LHV (kJ/kg) | 45,100 |
| Specific chemical exergy (kJ $kg^{-1}$) | 46,713 |
| Molar weight (kg $kmol^{-1}$) | 16.85 |
| *Air properties* [27] | |
| Composition (% by volume) | $N_2$ (78.09%), $O_2$ (20.95%), Ar (0.93%), $CO_2$ (0.03%) |
| Molar weight (kg $kmol^{-1}$) | 28.97 |

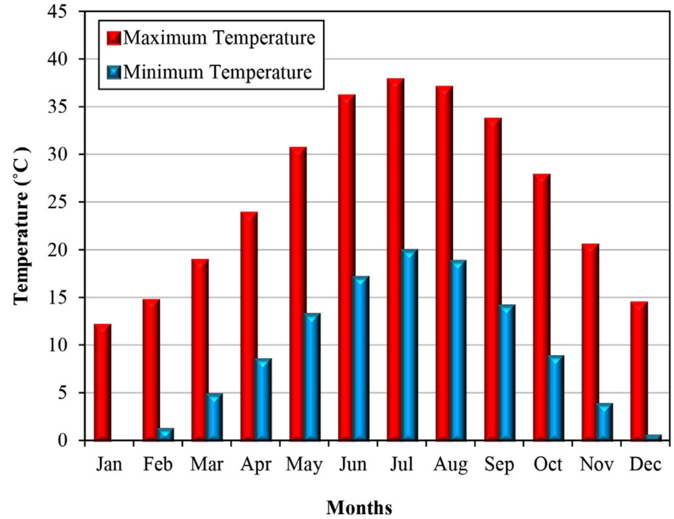


**Fig. 3.** Variation of the minimum and maximum values of ambient temperature in Shiraz over a typical year [49].

## 6. Results and discussion

### 6.1. Model verification

In order to validate the modeling results of gas turbine cycle, the main performance parameters of GT system including the thermal efficiency ($\eta_{th}$), the fuel mass flow rate ($\dot{m}_f$), and air mass flow rate ($\dot{m}_a$) obtained from the developed model are compared with the corresponding values given in Ref. [54]. As shown in Table 5, the mean difference value was less than 1.8%, which verifies the sufficient accuracy of the developed simulation code to model the thermal performance of the gas turbine system.

Furthermore, the basic parameters of the ITES system including the refrigerant mass flow rate ($\dot{m}_r$), the refrigeration compressor power consumption ($\dot{W}_{C2}$), and the coefficient of performance (COP) are obtained from the modeling results and compared with the corresponding values reported in Ref. [55] to ensure the accuracy of modeling. In this comparison, the relative difference is less

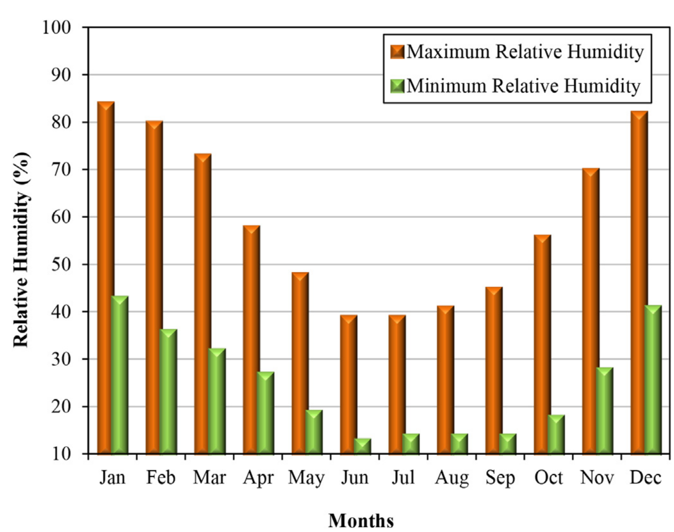


**Fig. 4.** Variation of the minimum and maximum values of relative humidity in Shiraz over a typical year [49].

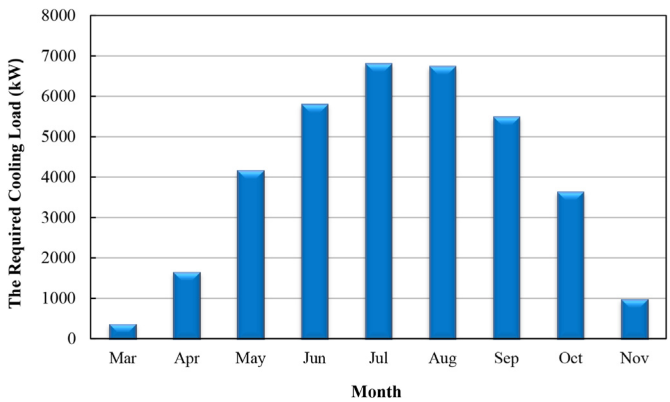


**Fig. 5.** The average cooling load required for each month of inlet air cooling for GT cycle in Shiraz.

than 1.5% (as shown in Table 6), which was deemed to be an acceptable value.

### 6.2. Optimization results

In the optimization procedure of the present study, 6 design parameters have been taken into account. Table 3 demonstrates the considered design parameters and their corresponding range of variations.

The tuning parameters for the genetic algorithm optimization procedure employed for optimization of the modeled system are presented in Table 7.

Fig. 6 demonstrates the Pareto optimal solutions achieved by applying the optimization procedure. The trend of the Pareto front evidently shows the previously mentioned conflict between the considered objective functions. Each point on the Pareto curve in Fig. 6 shows the possible optimal solutions which satisfy the objectives at an acceptable level without being dominated by any other solution. As shown in Fig. 6, the point A is the design leading to the highest possible exergetic efficiency (and accordingly, the highest cost). Point B is the design resulting in lowest possible exergetic efficiency (and thus, the lowest possible cost). It should be noted out that these represent lower and upper bounds for the design parameters. Thus, exergetic efficiencies higher than design point A or lower than point B cannot be achieved. Among the designs, the final chosen design point in the Pareto front is the one leading to the lowest possible total cost rate. That is, for any specific total cost rate, the chosen point of the Pareto front demonstrates the design with the highest possible exergetic efficiency.

As can be observed in this figure, increasing the exergetic efficiency up to about 33% does not significantly increase the total cost rate of the system while increasing it from 33% to 34% results in a moderate increase in the value of the other objective function. Any attempt to increase the exergetic efficiency above 34% leads to a severe increase in the total cost rate. This is due to the fact that as the exergetic efficiency exceeds 34%, the optimal decision variables (e.g. isentropic efficiencies of air compressor ($\eta_{C1}$) and gas turbine ($\eta_{GT}$)) near their thermodynamic upper bounds, which results in a dramatic increase in their corresponding capital costs. Furthermore, in order to decrease the rate of exergy destruction, the temperature difference across the evaporator and condenser shift to minimal values. This fact leads to a huge increase in heat transfer surface areas and subsequently a significant jump in capital costs of the evaporator, condenser, and the ice storage tank.

As demonstrated in Fig. 6, the design parameters of point A results in reaching the highest exergetic efficiency (34.53%) while leading to highest total cost rate (1.29964 US$ $s^{-1}$) Apparently, in case only the exergetic efficiency would be considered as the objective function, this point should be selected as the optimum design point. Conversely, in order to have the minimum value of the total cost rate (1.01347 US$ $s^{-1}$) of the system, the design point B can be selected; although this choice results in the lowest exergetic efficiency (29.87%). Accordingly, taking into account the total cost rate as the only objective function, the design point B should be selected as the optimal solution.

In a multi-criteria problem, a process of decision-making to select the final optimal solution from existing results is required. There are numerous approaches for decision-making process which can be applied to choose the final optimal solution from the

**Table 7**
The tuning parameters of the optimization program.

| Tuning parameters | Value |
|---|---|
| Population size | 300 |
| Maximum number of generations | 200 |
| Minimum function tolerance | $10^{-5}$ |
| Probability of crossover | 90% |
| Probability of mutation | 1% |
| Number of crossover point | 2 |
| Selection process | Tournament |
| Tournament size | 2 |

**Table 5**
Comparison of computed values of system operating parameters obtained from modeling of GT cycle system with the corresponding values reported in Ref. [54].

| Parameter | Unit | Modeling | Reported | Difference (%) |
|---|---|---|---|---|
| Thermal efficiency ($\eta_{th}$) | – | 35.8 | 35.2 | 1.7 |
| Fuel mass flow rate ($\dot{m}_f$) | kg $s^{-1}$ | 4.17 | 4.1 | 1.7 |
| Air mass flow rate ($\dot{m}_a$) | kg $s^{-1}$ | 184.4 | 188 | 1.9 |

**Table 6**
Comparison of the computed values of system performance parameters including the refrigerant mass flow rate ($\dot{m}_r$), the refrigeration compressor power consumption ($\dot{W}_{C2}$), and the coefficient of performance (COP) obtained from modeling of vapor compression refrigeration system desalination system with the corresponding values reported in Ref. [55].

| Input | | Output | Modeling | Reported | Difference (%) |
|---|---|---|---|---|---|
| $T_{EV}$ (°C) | −20 | $\dot{m}_r$ (kg $s^{-1}$) | 0.2001 | 0.2 | 0.05 |
| $T_{Cond}$ (°C) | 40 | $\dot{W}_{C2}$ (kW) | 9.1102 | 9 | 1.22 |
| $\dot{Q}_{EV}$ (kW) | 25.9 | COP | 2.8430 | 2.87 | 0.94 |

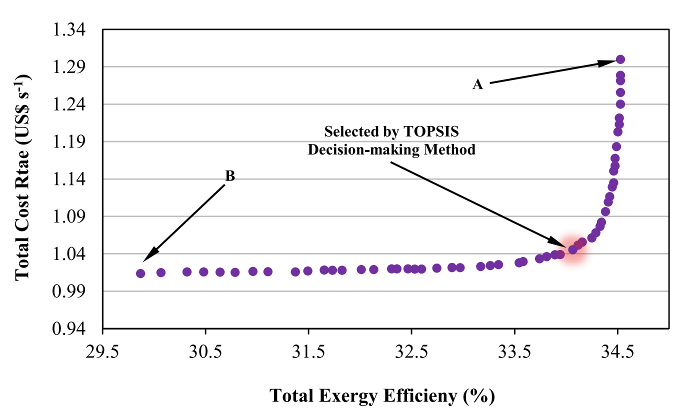


**Fig. 6.** Pareto optimal frontier from multi-objective optimization of the GT system with inlet air cooling.

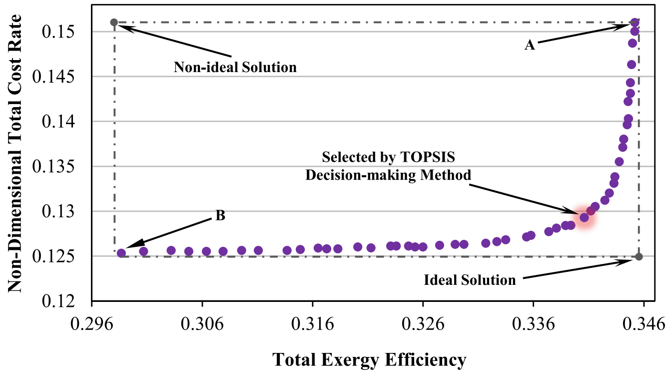


**Fig. 7.** The set of non-dimensional Pareto optimal solutions using the TOPSIS decision-making method to specify the final optimal design point of the GT system with inlet air cooling.

Pareto frontier. As the first step toward selecting the desired solution from available options, the values of objective functions should be non-dimensionalized. The non-dimensionalization method utilized in the present work is the Euclidian technique which was applied in Ref. [24] – details of this approach can also be found in Ref. [56]. After applying this method, all the non-dominated optimal solutions are converted to a non-dimensional form, which is demonstrated in Fig. 7.

After applying Euclidian non-dimensionalization to the objectives, decision making is performed using the TOPSIS (Technique for Order Preference by Similarity to an Ideal Solution) method to choose the final optimum design point. An ideal point is the solution with the best value for each objective function, while the non-ideal solution has the worst value for each objective among the values available in Pareto frontier [7]. In TOPSIS decision-making method, deviation of each solution from the ideal and non-ideal points is evaluated and the solution with minimum distance from the ideal point and maximum distance from the non-ideal solution is selected as the final optimal point [57]. Employing the TOPSIS decision-making method, a design point leading to exergetic efficiency of 34.06% and total cost rate of 1.04551US$ $s^{-1}$ is achieved as the final optimum solution. Fig. 7 demonstrates the chosen final optimal point while its corresponding optimal design parameters are given in Table 8. This table also demonstrates the values of the parameters of the design points which are achieved by performing single-objective optimization taking into account each of the considered objectives.

In order to demonstrate the location of exergy losses, the exergy destruction rate of each component is given in Table 9. These values are given for the optimal points achieved by the three methods of optimization including multi-objective optimization (by utilizing the explained selection method) and single-objective ones taking into account each objective function separately. According to this table, the highest amount of exergy destruction rate takes place in the combustion chamber (42.141 MW, 50.259 MW and 42.957 MW for maximizing objective function I (exergetic efficiency), minimizing objective function II (total cost rate), and multi-objective optimization respectively). The next highest exergy destruction rates occur at the recuperator, the gas turbine, and the air compressor. The practical utility of performing the exergetic analysis is in determining the location and true magnitude of exergy waste due to thermodynamic irreversibilities and inefficiencies. Such information can be useful to show the room for improvement and to identify specific components which limit the system. It was demonstrated in this work that the highest exergy destruction takes place in the combustion chamber – a relatively lower cost component. Thus, this study indicates that this component warrants substantial future research and development (in terms of fluid mechanics, materials science, and heat transfer) to improve its design and performance to achieve fully optimized inlet air cooling systems.

**Table 8**
The optimal values of system design parameters obtained from the three methods of optimization.

| Design parameter | Single-objective optimization (objective function I) | Single-objective optimization (objective function II) | Multi-objective optimization (objective functions I and II) |
|---|---|---|---|
| $r_{p,C1}$ | 13.6 | 10.4 | 11.9 |
| $\eta_{C1}$ (%) | 89.7 | 81.2 | 83.1 |
| $\eta_{GT}$ (%) | 90.9 | 81.0 | 84.7 |
| TIT (K) | 1317.9 | 1241.3 | 1279.5 |
| $T_{ST}$ (°C) | −5.8 | −3.7 | −4.6 |
| $T_{EV}$ (°C) | −7.7 | −5.9 | −6.7 |
| $T_{Cond}$ (°C) | 35.3 | 38.4 | 36.9 |

**Table 9**
Exergy destruction rate (in terms of MW) of various components in GT–ITES system at optimal points obtained from three methods of optimization.

| Component | Single-objective optimization (objective function I) | Single-objective optimization (objective function II) | Multi-objective optimization (objective functions I and II) |
|---|---|---|---|
| Air compressor | 3.454 | 3.871 | 3.503 |
| Recuperator | 5.748 | 6.537 | 5.836 |
| Combustion chamber | 42.141 | 50.259 | 42.957 |
| Gas turbine | 5.321 | 6.008 | 5.413 |
| Air cooler | 0.821 | 0.923 | 0.839 |
| Storage tank | 0.427 | 0.485 | 0.433 |
| Evaporator | 1.475 | 1.696 | 1.498 |
| Refrigeration compressor | 0.455 | 0.518 | 0.461 |
| Expansion valve | 0.0367 | 0.0421 | 0.0373 |
| Condenser | 0.878 | 1.007 | 0.892 |
| Cooling tower | 1.368 | 1.551 | 1.389 |

In order to have a better demonstration of the share of each component in the total capital cost, the corresponding capital costs are given in Fig. 8. Similar to Table 9, the values are given for three different optimal designs achieved from the mentioned optimization methods. As shown in this figure, the gas turbine requires the highest capital cost (5.3263, 4.1645 and 4.2964 MUS$ for single-objective I, II, and multi-objective optimization, respectively), while the next most costly components are the air compressor, the recuperator, the air cooler, and the refrigeration compressor, respectively.

The performance indicators of the system in optimal design points achieved using each of the mentioned optimization methods are listed in Table 10. The corresponding results of the single objective optimizations were previously discussed. By applying multi-objective optimization, a trade-off between the considered objectives is obtained and the exergetic efficiency of 34.06% is achieved.

In order to demonstrate the effect of fuel unit cost, the optimal design parameters achieved considering different values of fuel unit costs are reported in Table 11. Evidently, increasing the fuel unit cost makes changes optimal design parameters to reach a more thermodynamically efficient design. The same trend can also been in Fig. 9 which demonstrates the effect of variation in the unit cost of fuel on the achieved Pareto front. By increasing the unit cost of fuel, the Pareto optimal solutions move leftward (higher exergetic efficiency) and upward (higher total cost) simultaneously. It should

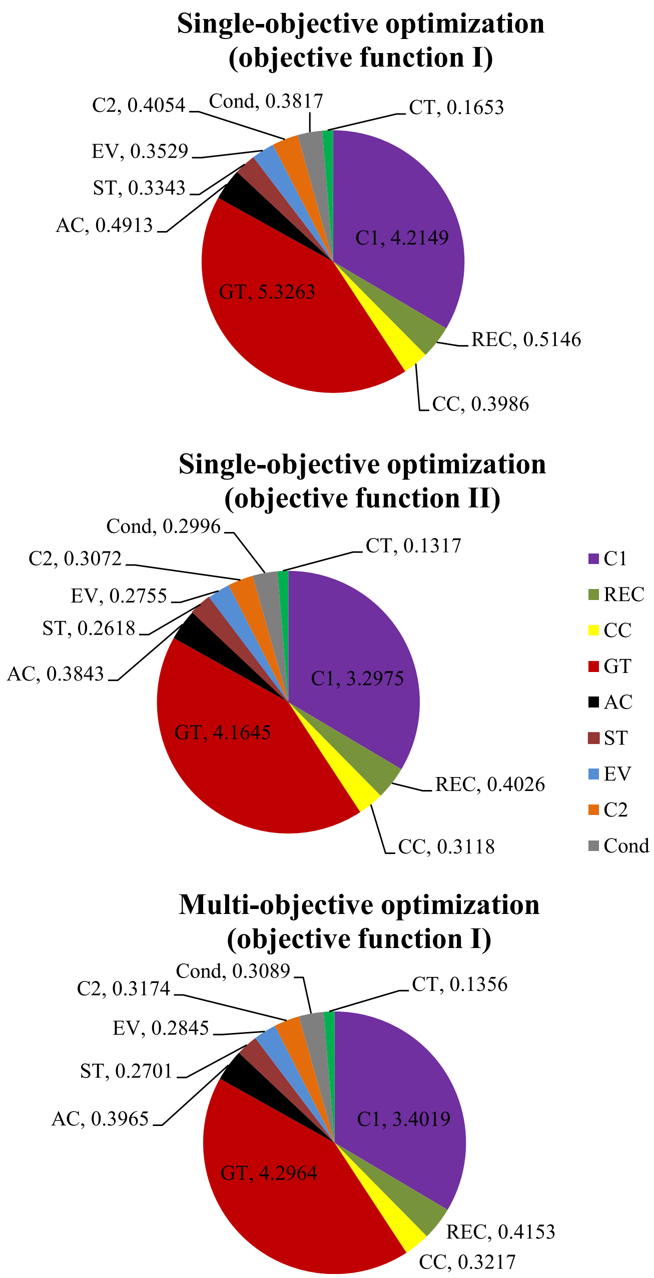


**Fig. 8.** Capital costs (in terms of MUS$) of various system components at optimal points obtained from three methods of optimization.

be noted that the he upward movement of the Pareto optimal solutions is due to increases in the total cost rate of the system. It is also noteworthy that the sensitivity of the optimal solutions to the fuel cost is much higher at the points leading to lower exergetic efficiencies than the ones with higher exergetic efficiencies.

The payback period for additional investment of the cycle (ITES system) is a very important factor for assessment of the modeled system. Thus, values of the payback period for gas turbines with nominal power output of 25–150 MW are estimated and presented in Fig. 10. According to Fig. 10, the estimated payback period for the mentioned ranges of gas turbine power outputs changes from about 2.31 to 7.04 years. For our case study, the value of payback period is estimated to be 4.72 years. The payback period obtained by Sanaye et al. [11] for a similar system was 6.5 years and the one evaluated by Ameri et al. [58] was 5.55 – both are higher than the present work. The difference is due to the fact these studies are located in the cities which are considerably warmer than the present study. A warmer climate necessitates a higher cooling load and cooling capacity, resulting in higher payback periods. Fig. 10 also shows that the slope of increase in payback period decreases as the net power output of gas turbine increases. It should be pointed out that the trend obtained from our study is very close to the one presented by Sanaye et al. [11]. Therefore, the additional investment cost imposed by the installation of ITES system can be compensated in less than 5 years with the income received from selling the extra power generated from inlet air cooling.

**Table 10**
Performance-related results of GT–ITES system at optimal points obtained from three methods of optimization.

| Parameter | Single-objective optimization (objective function I) | Single-objective optimization (objective function II) | Multi-objective optimization (objective functions I and II) |
|---|---|---|---|
| Net power output (MW) | 63.5 | 55.3 | 60.8 |
| $CO_2$ emission (kg $y^{-1}$) | $333.474 \times 10^6$ | $405.484 \times 10^6$ | $343.762 \times 10^6$ |
| CO emission (kg $y^{-1}$) | $322.752 \times 10^3$ | $353.028 \times 10^3$ | $329.594 \times 10^3$ |
| $NO_x$ emission (kg $y^{-1}$) | $8.083 \times 10^3$ | $9.014 \times 10^3$ | $8.382 \times 10^3$ |
| Social cost of air pollution (MUS$ $y^{-1}$) | 7.5319 | 9.1520 | 7.7646 |
| Refrigeration system COP | 4.441 | 4.279 | 4.367 |
| Total exergy efficiency (%) | 34.53 | 29.87 | 34.06 |
| Total annual cost (MUS$) | 35.6712 | 27.8167 | 28.6961 |

**Table 11**
The sensitivity analysis of change in the numerical values of optimal design parameters of GT–ITES system with variation in fuel unit cost.

| Change in the values of design parameters | Variation in fuel unit cost | | | |
|---|---|---|---|---|
| | −50% | −25% | +25% | +50% |
| $\Delta r_{p,C1}/r_{p,C1}$ | −3.94% | −2.51% | +2.16% | +3.81% |
| $\Delta\eta_{C1}/\eta_{C1}$ | −4.86% | −2.91% | +3.18% | +5.22% |
| $\Delta\eta_{GT}/\eta_{GT}$ | −5.74% | −3.01% | +2.74% | +5.12% |
| $\Delta(TIT)/TIT$ | +2.04% | +1.14% | −1.07% | −1.84% |
| $\Delta T_{ST}/T_{ST}$ | −3.87% | −1.94% | +2.18% | +4.25% |
| $\Delta T_{EV}/T_{EV}$ | −3.79% | −1.83% | +2.09% | +4.17% |
| $\Delta T_{Cond}/T_{Cond}$ | +2.46% | +1.31% | −1.09% | −1.95% |

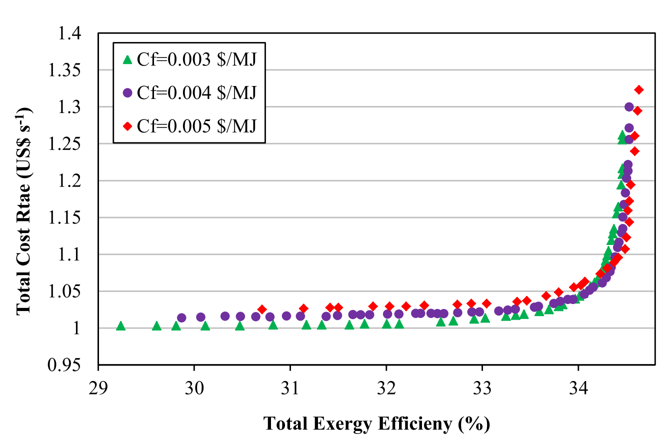


**Fig. 9.** Sensitivity of Pareto optimal solutions to the fuel unit cost.

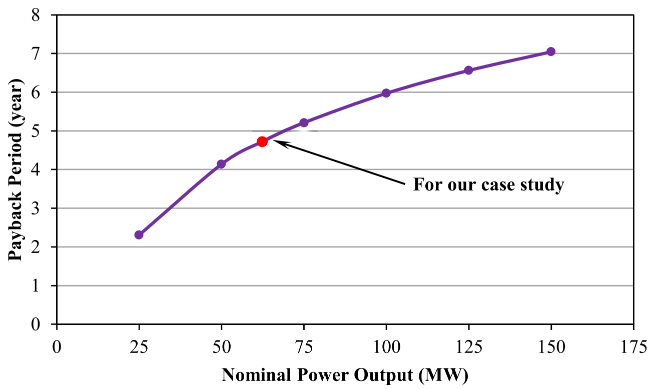


**Fig. 10.** Payback period of additional investment for the gas turbine system due to inlet air cooling using ITES system.

## 7. Conclusions

In the present work, ITES system for GT cycle inlet air cooling was mathematically modeled and analyzed from energetic, exergetic, economic, and environmental (emissions cost) framework. Employing multi-objective genetic algorithm, the system was optimized while considering exergetic efficiency and total cost rate of the system as objectives. Consequently, a set of optimal solutions is achieved and by employing a specific selection method, the final optimal design point is chosen. The optimal parameters achieved by utilizing the mentioned multi-objective method and also single objective approach considering each of the objective functions are compared. Single objective optimization of the system only in order to maximize the exergetic efficiency leads to a design which results in a total cost of 35.6712 MUS$ while reaching the exergetic efficiency of 34.53%. Optimizing the system in order to minimize the cost as the single objective results in the exergetic efficiency of 29.87% while leading to total cost of 27.8167MUS$. By performing the multi objective optimization and the mentioned selection method a design leading to exergetic efficiency of 34.06% and total cost of 28.6961 MUS$ is achieved. The results demonstrate that the multi-objective optimization has provided a reasonable trade-off between the two objectives.

Finally, the optimization results showed that the ITES system used for inlet air cooling increased the power output by 11.63% and the exergetic efficiency of the system by 3.59%, while the extra costs associated with using ITES system is compensated with the income received from selling the increased generated electrical power in 4.72 years.

## Acknowledgments

The authors would like to acknowledge the CRC for Low Carbon Living for providing scholarship support to A. Shirazi.

## References


[1] Mahmoudi SMS, Zare V, Ranjiban F, Garooci Farshi L. Energy and exergy analysis of simple and regenerative gas turbine inlet air cooling using absorption refrigeration. J Appl Sci 2009;9:2399–407.
[2] Farzaneh-Gord M, Deymi-Dashtebayaz M. Effect of various inlet air cooling methods on gas turbine performance. Energy 2011;36(2):1196–205.
[3] Shi X, Agnew B, Che D, Gao J. Performance enhancement of conventional combined cycle power plant by inlet air cooling, inter-cooling and LNG cold energy utilization. Appl Therm Eng 2010;30(14–15):2003–10.
[4] Sadrameli SM, Goswami DY. Optimum operating conditions for a combined power and cooling thermodynamic cycle. Appl Energy 2007;84(3):254–65.
[5] Zurigat YH, Dawoud B, Bortmany J. On the technical feasibility of gas turbine inlet air cooling utilizing thermal energy storage. Int J Energy Res 2006;30(5):291–305.
[6] Zadpoor AA, Golshan AH. Performance improvement of a gas turbine cycle by using a desiccant-based evaporative cooling system. Energy 2006;31(14):2652–64.
[7] Sanaye S, Shirazi A. Four E analysis and multi-objective optimization of an ice thermal energy storage for air-conditioning applications. Int J Refrigeration 2012;36(3):828–41.
[8] Dincer I. On thermal energy storage systems and applications in buildings. Energy Build 2002;34(4):377–88.
[9] Tan H, Li Y, Tuo H, Zhou M, Tian B. Experimental study on liquid/solid phase change for cold energy storage of liquefied natural gas (LNG) refrigerated vehicle. Energy 2010;35(5):1927–35.
[10] Sanaye S, Shirazi A. Thermo-economic optimization of an ice thermal energy storage system for air-conditioning applications. Energy Build 2012;60:100–9.
[11] Sanaye S, Fardad A, Mostakhdemi M. Thermoeconomic optimization of an ice thermal storage system for gas turbine inlet cooling. Energy 2011;36(2):1057–67.
[12] Saito A. Recent advances in research on cold thermal energy storage. Int J Refrigeration 2002;25(2):177–89.
[13] Li G, Hwang Y, Radermacher R, Chun H-H. Review of cold storage materials for subzero applications. Energy 2013;51:1–17.
[14] Ezan MA, Erek A, Dincer I. Energy and exergy analyses of an ice-on-coil thermal energy storage system. Energy 2011;36(11):6375–86.
[15] Al-Ibrahim AM, Varnham A. A review of inlet air-cooling technologies for enhancing the performance of combustion turbines in Saudi Arabia. Appl Therm Eng 2010;30(14–15):1879–88.
[16] Habeebullah BA. Economic feasibility of thermal energy storage systems. Energy Build 2007;39(3):355–63.
[17] Mohanty B, Paloso Jr G. Enhancing gas turbine performance by intake air cooling using an absorption chiller. Heat Recovery Syst CHP 1995;15(1):41–50.
[18] Ameri M, Hejazi SH. The study of capacity enhancement of the Chabahar gas turbine installation using an absorption chiller. Appl Therm Eng 2004;24(1):59–68.
[19] Khaliq A, Dincer I. Energetic and exergetic performance analyses of a combined heat and power plant with absorption inlet cooling and evaporative aftercooling. Energy 2011;36(5):2662–70.
[20] Ehyaei MA, Hakimzadeh S, Enadi N, Ahmadi P. Exergy, economic and environment (3E) analysis of absorption chiller inlet air cooler used in gas turbine power plants. Int J Energy Res 2012;36(4):486–98.
[21] Najafi Behzad, Shirazi Ali, Aminyavari Mehdi, Rinaldi Fabio, Taylor RA. Exergetic, economic and environmental analyses and multi-objective optimization of an SOFC-gas turbine hybrid cycle coupled with an MSF desalination system. Desalination 2014;334:46–59.
[22] MacPhee D, Dincer I. Performance assessment of some ice TES systems. Int J Therm Sci 2009;48(12):2288–99.
[23] Shirazi A, Aminyavari M, Najafi B, Rinaldi F, Razaghi M. Thermal–economic–environmental analysis and multi-objective optimization of an internal-reforming solid oxide fuel cell–gas turbine hybrid system. Int J Hydrogen Energy 2012;37(24):19111–24.
[24] Navidbakhsh M, Shirazi A, Sanaye S. Four E analysis and multi-objective optimization of an ice storage system incorporating PCM as the partial cold storage for air-conditioning applications. Appl Therm Eng 2013;58(1–2):30–41.
[25] ASHRAE handbook: fundamentals. Atlanta, USA: ASHRAE; 2009.
[26] Kakac S, Liu H. Heat exchangers: selection, rating and thermal design. 2nd ed. Washington DC, USA: Boca Raton; 2002. Fla.: CRC Press.
[27] Kotas TJ. The exergy method of thermal plant analysis. Florida, USA: Malabar; 1995. Fla.: Krieger Pub.
[28] Bloch HP, Hoefner JJ. Reciprocating compressors – operation and maintenance. Woburn, USA: Butterworth-Heinemann; 1996.
[29] ASHRAE handbook: HVAC systems and equipment. Atlanta, USA: ASHRAE; 2008.
[30] Söylemez MS. On the optimum sizing of cooling towers. Energy Convers Manag 2001;42(7):783–9.
[31] Bejan A, Tsatsaronis G, Moran M. Thermal design and optimization. New York, USA: John Wiley and Sons; 1996.
[32] Sayyaadi H. Multi-objective approach in thermoenvironomic optimization of a benchmark cogeneration system. Appl Energy 2009;86(6):867–79.
[33] Roosen P, Uhlenbruck S, Lucas K. Pareto optimization of a combined cycle power system as a decision support tool for trading off investment vs. operating costs. Int J Therm Sci 2003;42(6):553–60.
[34] Wall G. Optimization of refrigeration machinery. Int J Refrigeration 1991;14(6):336–40.
[35] Selbaş R, Kızılkan Ö, Şencan A. Thermoeconomic optimization of subcooled and superheated vapor compression refrigeration cycle. Energy 2006;31(12):2108–28.
[36] Panjeshahi MH, Ataei A. Application of an environmentally optimum cooling water system design in water and energy conservation. Int J Environ Sci Technol 2008;5(2):251–62.
[37] Smith R. Chemical process design and integration. 2nd ed. New York, USA: John Wiley & Sons; 2005.
[38] Rizk NK, Mongia HC. Semi analytical correlations for NOx, CO and UHC emissions. J Eng Gas Turb Power 1993;115(3):612–29.
[39] Gulder OL. Flame temperature estimation of conventional and future jet fuels. J Eng Gas Turb Power 1986;108(2):376–80.

[40] Najafi H, Najafi B. Multi-objective optimization of a plate and frame heat exchanger via genetic algorithm. Heat Mass Transfer 2010;46(6):639–47.
[41] Selleri T, Najafi B, Rinaldi F, Colombo G. Mathematical modeling and multi-objective optimization of a mini-channel heat exchanger via genetic algorithm. J Therm Sci Eng Appl 2013;5(3):1–10.
[42] Najafi B, Najafi H, Idalik MD. Computational fluid dynamics investigation and multi-objective optimization of an engine air-cooling system using a genetic algorithm. Proc Inst Mech Eng C: J Mech Eng Sci 2011;225(6):1389–98.
[43] Najafi H, Najafi B, Hoseinpoori P. Energy and cost optimization of a plate and fin heat exchanger using genetic algorithm. Appl Therm Eng 2011;31(10):1839–47.
[44] Konak A, Coit DW, Smith AE. Multi-objective optimization using genetic algorithms: a tutorial. Reliab Eng Syst Saf 2006;91(9):992–1007.
[45] Ahmadi P, Dincer I. Exergoenvironmental analysis and optimization of a cogeneration plant system using multimodal genetic algorithm (MGA). Energy 2010;35(12):5161–72.
[46] Ansari K, Sayyaadi H, Amidpour M. Thermoeconomic optimization of a hybrid pressurized water reactor (PWR) power plant coupled to a multi effect distillation desalination system with thermo-vapor compressor (MED-TVC). Energy 2010;35(5):1981–96.
[47] Mossolly M, Ghali K, Ghaddar N. Optimal control strategy for a multi-zone air conditioning system using a genetic algorithm. Energy 2009;34(1):58–66.
[48] Aminyavari M, Najafi B, Shirazi A, Rinaldi F. Exergetic, economic and environmental (3E) analyses, and multi-objective optimization of a $CO_2/NH_3$ cascade refrigeration system. Appl Therm Eng 2014;65:42–50.
[49] World Weather Information Service. Weather information for Shiraz. URL: www.worldweather.org/114/c00936.htm; 2013 [accessed 21.12.13].
[50] Malcolm W. NIST-JANAF thermodynamic tables part 1 and 2. 4th ed. New York, USA: Am. Chem. Soc. Am. Inst. Phys.; 1989.
[51] US Department of Energy. Social cost of carbon for regulatory impact analysis under executive order 12866. URL: www1.eere.energy.gov/buildings/appliance_standards/residential/pdfs/hvac_app_16-a_social_cost_carbon_2011-04-25.pdf; 2012 [accessed 21.12.13].
[52] Lazzaretto A, Toffolo A. Energy, economy and environment as objectives in multi-criterion optimization of thermal systems design. Energy 2004;29(8):1139–57.
[53] Iranian Central Bank. URL: www.cbi.ir; 2011 [accessed 21.12.13].
[54] Bhargava R, Meher-Homji CB. Parametric analysis of existing gas turbines with inlet evaporative and overspray fogging. J Eng Gas Turb Power 2005;127(1):145–58.
[55] Dincer I. Refrigeration systems and applications. West Sussex: John Wiley & Sons; 2003.
[56] Sayyaadi H, Mehrabipour R. Efficiency enhancement of a gas turbine cycle using an optimized tubular recuperative heat exchanger. Energy 2012;38(1):362–75.
[57] Yue Z. A method for group decision-making based on determining weights of decision makers using TOPSIS. Appl Math Model 2011;35(4):1926–36.
[58] Ameri M, Hejazi SH, Montaser K. Performance and economic of the thermal energy storage systems to enhance the peaking capacity of the gas turbines. Appl Therm Eng 2005;25(2–3):241–51.